TIME-RESOLVED MEASUREMENTS OF HIGH-FIELD QUENCH IN SRF CAVITIES

S. Antipov, University of Chicago, Chicago, IL, USA
E.Efimenko, Moscow Institute of Physics and Technology, Russia
A. Romanenko, Dmitri Sergatskov, FNAL, Batavia, IL, USA

Abstract

Fermilab temperature mapping system for SRF cavities has been improved to operate with time resolution of <1ms. Using the improved system, quench dynamics has been investigated in several cavities. It has been determined that the maximal size of a normal conducting zone during quench can be as high as 130 mm, its growth rate – 20 mm/ms, and temperature inside – up to 40 K; cavities recover after quench within 100 – 250 ms. Findings are consistent with the thermal breakdown mechanism.

INTRODUCTION

In SRF cavities "quench" is a local loss of a superconducting state leading to a rapid decrease of the stored energy. Quench is one of the main factors limiting achievable gradients. While low-field (E_{acc} < 20 MV/m) quenches are typically caused by apparent large defects, at the moment there is no clear understanding of the nature of the defects that cause quench at high fields (E_{acc} > 20 MV/m). There are two plausible mechanisms of the high-field quench: thermal breakdown and thermo-magnetic breakdown [1]. Thermal breakdown is though to be triggered by the defect that has a surface resistance greater than surrounding niobium, whereas in a thermo-magnetic breakdown, the defect has a lower RF critical magnetic field. This difference leads to a different triggering mechanism, and hence different initial propagation conditions, which may influence the evolution of the process. Consequently understanding dynamics of quench gives a clue to underlying physics and the nature of quench.

In this paper we present results of measuring quench dynamics using time-resolved temperature mapping. It allows to observe and measure the evolution of the size of normal conducting region and temperature distribution within it.

EXPERIMENTAL SETUP

The experiment was held at Fermilab using TESLA shape SRF cavities with the fundamental TM_{010} mode at the frequency of 1.3 GHz. Measurements were performed at the Fermilab Vertical Test Stand [2] at temperatures down to 1.5 K. Fermilab full body temperature mapping system, which is based on the design similar to a system at Jefferson Lab [3,4], has been used for the studies. In such a system temperature sensors are 100 Ω carbon Allen-Bradley resistors, whose resistance decreases exponentially with temperature. These thermometers are fixed on 36 printed circuit boards (PCBs), 16 thermometers on each. The shape of PCBs replicates the shape of ILC TESLA shape 1.3 GHz cavities. PCBs are placed every 10 degrees around cavity rotational axis. Horizontal distance between thermometers is about 18 mm on cavity equator and is smaller further away; vertical spacing is about 10 mm (Figure 1).

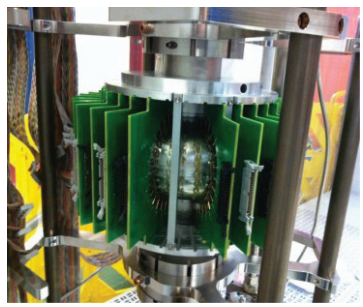

Figure 1: Fermilab temperature mapping assembled on the single cell niobium cavity.

Carbon resistors are connected in parallel to a Keithley 2400 voltage source, providing 10 V DC. Each thermometer is connected in series to two 1 MΩ resistors. This scheme provides a 5 μA constant current through carbon resistors. Measurement of voltage drop across them gives their resistance R, which is then converted into temperature T. Calibration curves for R-T conversion are obtained on each of the system cool down cycles from 4.2 to 1.6 K.

Data acquisition from all 576 thermometers is performed by two SCXI-1001 chassis that contain 18 SCXI-1102 modules. Each module is capable of multiplexing 32 channels, collects data from two PCBs, and provides a maximum sampling rate of 333 kHz. Analog signal from them is routed to a computer which performs analog to digital conversion. The maximum rate of conversion is 333 kHz. Operation of SCXI modules is controlled by a LabVIEW program.

For the purpose of obtaining a full T-map temperature is measured in a following way. First, a measurement without field is made to get the background temperature distribution. Then several measurements are made with different polarities of source signal, and the results are averaged. This technique provides precise measurements of temperature, with up to ~50 microK resolution possible. The down side is that the procedure takes too much time – obtaining a full temperature map takes about

ISBN 978-3-95450-143-4

a second, which is significantly greater than typical times of quench – tens of milliseconds.

To increase data acquisition rate one may select a subset of thermometers to be measured from a whole array and perform only one measurement of each sensor. In this case the maximum sampling rate F_s is limited by hardware performance, namely by maximum sampling rate of SCXI modules and the fact that they cannot skip unused channels. Maximal F_s was observed to be approximately equal to $F_s = 10 / N$ kHz, where N is the total number of SCXI modules, used in creating a temperature map.

EXPERIMENTAL PROCEDURE

The experimental procedure was the following: first, measure the quality factor of the cavity, increasing the amount of stored energy, to find the critical accelerating gradient; then perform a full temperature map, using all thermometers, to localize the quench; and finally, perform time-resolved measurements of temperature distribution in quench region, taking data only from a small number of thermometers, but with high sampling rate.

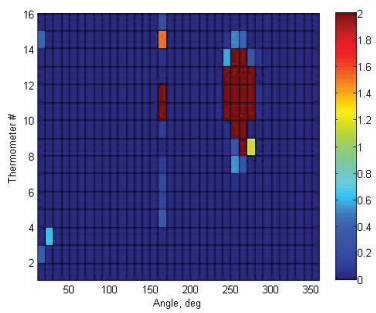

Figure 2: Temperature map. Cavity TE1NR005, field 22.3 MV/m. Thermoboard at 160° is faulty due to broken cable connector.

Figure 2 depicts a typical quench image, obtained by full temperature mapping. The map is not continuous, because obtaining a full temperature map takes roughly a second, so different pieces of the picture were taken at different moments of time. Nevertheless, one can notice a hot region produced by quench. Knowing the position of the hot spot, a subset of thermometers around it was picked to be measured with sampling rate of 10 kHz. The resulting data had a lot of high frequency noise, most probably coming fromt the electrical circuit. To filter the noise, the data was averaged with 1 ms intervals. Data in faulty channels was approximated by linear fits using the data from adjacent channels. A smoothed picture of the resulting signal is depicted in Figure 3.

RESULTS

We tested 3 ILC-type 1.3 GHz cavities: TE1NR005, TE1AES003, and TE1ACC005 at the temperature of 2 K. Treatments of the cavities were different – all of them were electropolished and baked at 120° C, but TE1AES003 was also subjected to furnace nitrogen treatment [5]. Quenches happened in a wide range of the accelerating field strength from 20 to 33 MV/m (Figure 4). In addition, cavity TE1AES003 was tested at two more temperatures: 1.8 and 2.165 K. The results are summarized in Table 1.

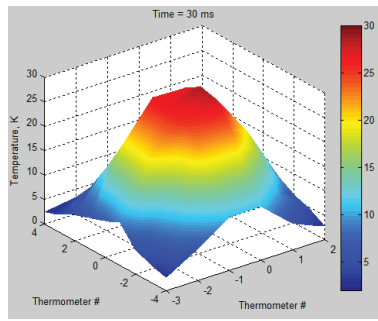

Figure 3: Temperature distribution on a cavity wall 30 ms after the quench started. Color corresponds to the deviation from $T_{He} = 2$ K.

Figure 5a) depicts the evolution of temperature in the center of the quench spot in TE1NR005 cavity with 1 ms time resolution. After the process starts the temperature rapidly increases from $T_{He} = 2K$ to about 30 K in 30 ms and then slowly decreases due to cooling by He; at $t_{SC} = 90$ ms the cavity returns to superconducting state. The rate of temperature increase at the beginning of the process is 2 K/ms.

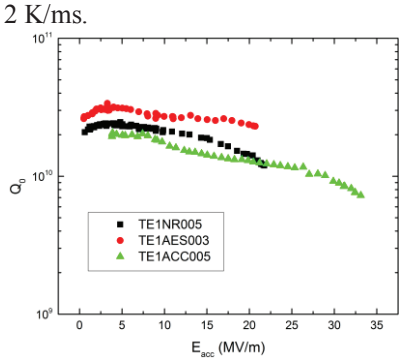

Figure 4: Quality factor vs accelerating gradient.

Another thing one can analyze is the radius of the normal zone. Its lower estimate is the distance from the center to the farthest thermometer with $T > T_C$. When a temperature on a thermometer passes the Nb transition temperature 9.2 K, the radius is exactly equal to the distance to that sensor. Figure 5b) depicts the dependence of quench radius on time with 1 ms time resolution. At the beginning the size of the hot spot increases with a rate of 18 mm/ms. The maximal radius of the hot spot is about 45 mm, which is consistent with the results of observations of quench by fast thermometry technique with 16 sensors, placed around cavity equator every 40 mm (Fig. 6). The estimated maximal diameter of the hot spot, obtained by that method, is 80 – 120 mm for $E_{acc} = 20 - 35$ MV/. Our data also agrees with simulation results for thermal breakdown [6].

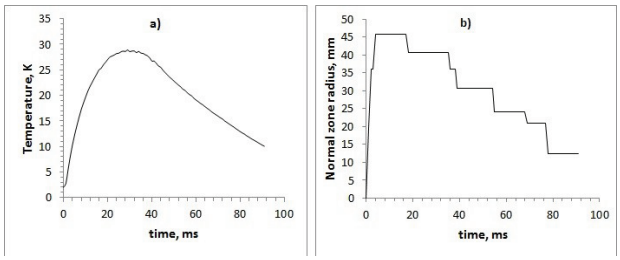

Figure 5: Temperature in the center of the hot spot – a) and its size – b) as a function of time. Cavity TE1NR005, quenching gradient 22.3 MV/m.

Table 1: Results. Cavity A – TE1AES003, B – TE1NR005, C – TE1ACC005

Cavity	A	A	A	B	C
T_{He}, K	1.8	2.0	2.165	2.0	2.0
Field, MV/m	20.7	21.7	21.6	22.3	33
Max R, mm	50	40	65	45	60
Max T, K	35	35	40	30	40
Growth rate, mm/ms	20	20	20	18	12
T increase rate, K/ms	2.5	2.3	2.3	2.4	2.5
t_{SC}, ms	105	110	190	90	250

As can be seen in Table 1 a quench, happening at a higher field, has greater temperature and size of hot spot, than the one at a lower one. Comparatively low value of T_{max} for TE1NR005 can be explained by the fact that the center of the hot spot, where the temperature is the greatest, was exactly in the middle between two thermometers, so the measured maximal temperature is lower than the actual one. It also takes cavity with greater quench field more time to return to a superconducting state – up to 250 ms for quench at 33 MV/m. These results are intuitive – the more energy stored into cavity is converted into heat the bigger and hotter spot appears.

The process of the initial growth of the normal conducting region does not seem to depend on the field or on the temperature of He bath. The rate of increase of the size of normal conducting zone and the rate of increase of temperature in its center are about 20 mm/ms and 2.5 K/ms correspondingly for all 6 cases. This result is important for numerical simulations of the process, since the cooling model is rather complex.

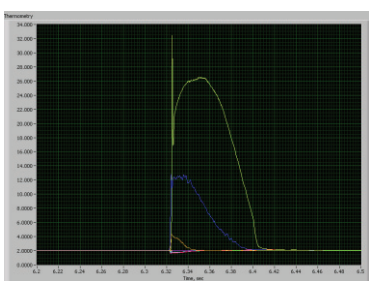

Figure 6: Thermometry detects 3 peaks on sensors spaced by 4 cm. Spot size is roughly 12 cm. E_{acc} = 30 MV/m.

In Figure 7 behavior at temperatures 1.8 K, 2.0 K, and 2.165 K is compared; the last one is close to He lambda point (where superfluid He II transitions to normal fluid He I, about 2.17 K), and the cooling in that case was significantly lower than in the first two. Plots for all three cases follow each other closely until 12 ms. This fact can be explained by spreading of the heat from the inner cavity wall, where the energy is dissipated. Because the temperature distribution on the inner wall at the beginning of the process is unaffected by helium cooling, it depends only on the field, which was roughly the same in all three cases. Thus, at first, the same temperature distribution appears on the outer wall and later it starts cooling down by He. Consequently, one can disregard cooling for the first 10 ms, when simulating quench.

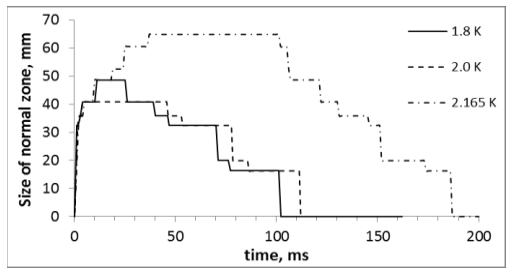

Figure 7: Evolution of quench radius over time for 3 different He temperatures: 1.8, 2.0, 2.165 K.

CONCLUSION

Experimental procedure, implemented on Fermilab's temperature mapping system, allows to measure temperature distribution within quench spot, as well as the amount of energy stored in the SRF cavity, at the moment when quench starts, during its growth, and decay with temporal resolution of 1ms.

Typical temporal parameters of the breakdown have been determined. For three tested SRF cavities, quenching at fields 20.7 – 33 MV/m, maximal radius of the normal zone was 40 – 65; time to return to superconducting state: 90 – 250 ms. The behavior of quench at the times lower than 10 ms has been observed to be independent on the stored energy and the amount of He cooling. Results on maximal radius of the normal zone are consistent with observations of quench by other techniques.

The experimental procedure can also be useful for investigating how different surface treatments affect the breakdown. Achieved results can be useful for better understanding of the nature of high-field quench, improvement of quench detection techniques, and material science research for future SRF cavities.

ACKNOWLEDGEMENTS

Authors are deeply indebted to R. Pilipenko for his help with digital signal processing.

REFERENCES

[1] R. L. Geng, Proceedings of SRF'11, Chicago, 2011, MOIOB06.

[2] J. P. Ozelis et al, Proceedings of PAC'07, 2007, WEPMN106.

ISBN 978-3-95450-143-4

[3] G. Ciovati et al., JLab Technical Note TN-05-59, 2005.
[4] J. Knobloch et al, Rev. Sci. Instrum. 65 (ll), 1994
[5] A. Grassellino et al, Supercond. Sci. Technol. 26 (2013) 102001.
[6] D. Sergatskov et al, Proceedings of SRF'13, Paris, 2013.

ISBN 978-3-95450-143-4